# CD206 + macrophages are relevant non-invasive imaging biomarkers and therapeutic targets in experimental lung fibrosis

Lenny Pommerolle, Guillaume Beltramo, Leo Biziorek, Marin Truchi, Alexandre Magno Maneschy Dias, Lucile Dondaine, Julie Tanguy, Nicolas Pernet, Victor Goncalves, Alexanne Bouchard, et al.

OPEN ACCESS

Original research

# CD206$^+$ macrophages are relevant non-invasive imaging biomarkers and therapeutic targets in experimental lung fibrosis

Lenny Pommerolle,[1] Guillaume Beltramo ,[1,2,3,4] Leo Biziorek,[1] Marin Truchi,[5] Alexandre Magno Maneschy Dias,[6] Lucile Dondaine,[1,3] Julie Tanguy,[1] Nicolas Pernet,[4] Victor Goncalves,[7] Alexanne Bouchard,[6] Marie Monterrat,[6] Grégoire Savary,[8] Nicolas Pottier,[8] Kjetil Ask,[9] Martin R J Kolb,[9] Bernard Mari,[5] Carmen Garrido,[1,3,6] Bertrand Collin,[6,7] Philippe Bonniaud,[1,2,3,4] Olivier Burgy,[1,3,4] Françoise Goirand,[1,3,4] Pierre-Simon Bellaye [1,3,6]

► Additional supplemental material is published online only. To view, please visit the journal online (https://doi.org/10.1136/thorax-2023-221168).

For numbered affiliations see end of article.

**Correspondence to**
Dr Philippe Bonniaud;
philippe.bonniaud@chu-dijon.fr

OB, FG and P-SB contributed equally.
LP and GB contributed equally.

Received 6 November 2023
Accepted 25 June 2024
Published Online First
20 July 2024

## ABSTRACT

**Background** Interstitial lung diseases (ILDs) include a large number of diseases associated with progressive pulmonary fibrosis (PPF), including idiopathic pulmonary fibrosis (IPF). Despite the rarity of each of the fibrotic ILDs individually, they cumulatively affect a considerable number of patients. PPF is characterised by an excessive collagen deposition leading to functional decline.

**Objectives** Therapeutic options are limited to nintedanib and pirfenidone which are only able to reduce fibrosis progression. CD206-expressing M2 macrophages are involved in fibrosis progression, and whether they may be relevant therapeutic targets or biomarkers remains an open question.

**Results** In our study, CD206$^+$ lung macrophages were monitored in bleomycin-induced lung fibrosis in mice by combining flow cytometry, scRNAseq and in vivo molecular imaging using a single photon emission computed tomography (SPECT) radiopharmaceutical, $^{99m}$Tc-tilmanocept. The antifibrotic effect of the inhibition of M2 macrophage polarisation with a JAK inhibitor, tofacitinib, was assessed in vivo. We demonstrate that CD206-targeted in vivo SPECT imaging with $^{99m}$Tc-tilmanocept was able to accurately detect and quantify the increase in CD206$^+$ macrophages from early to advanced stages of experimental fibrosis and ex vivo in lung biopsies from patients with IPF. CD206-targeted imaging also specifically detected a decrease in CD206$^+$ lung macrophages on nintedanib and tofacitinib treatment. Importantly, early in vivo imaging of CD206$^+$ macrophages allowed the prediction of experimental lung fibrosis progression as well as nintedanib and tofacitinib efficacy.

**Conclusions** These findings indicate that M2 macrophages may be relevant theranostic targets for personalised medicine for patients with PPF.

### WHAT IS ALREADY KNOWN ON THIS TOPIC

⇒ Prediction of disease progression and therapy efficacy remain a clinical issues in progressive pulmonary fibrosis (PPF).
⇒ Macrophages expressing CD206 on their surface have been recently described as profibrotic cells involved in the physiopathology of PPF.
⇒ Whether CD206$^+$ macrophages could be relevant biomarkers and/or therapeutic targets in lung fibrosis remains to be determined.

### WHAT THIS STUDY ADDS

⇒ Our study demonstrate for the first time that in vivo CD206-targeted molecular imaging with the radiopharmaceutical $^{99m}$Tc-tilmanocept is able to accurately detect and quantify the increase in CD206$^+$ cells in experimental lung fibrosis.
⇒ Most importantly, CD206-targeted imaging is able to predict lung fibrosis progression as well as the efficacy of existing and prospective antifibrotic drugs, such as nintedanib and tofacitinib.

### HOW THIS STUDY MIGHT AFFECT RESEARCH, PRACTICE OR POLICY

⇒ Our findings represent the first step towards the personalised management of patients with PPF with a non-invasive imaging tool able to select patients with high CD206$^+$ cell infiltration in the lungs for the use of anti-CD206 therapies such as tofacitinib and for potentially evaluating the efficacy of nintedanib during treatment.



**To cite:** Pommerolle L, Beltramo G, Biziorek L, *et al*. *Thorax* 2024;**79**:1124–1135.

## INTRODUCTION

Diffuse interstitial lung diseases (ILDs) include a large number of different diseases and causes, representing a significant burden of disease, with variable outcomes, possibly associated with progressive fibrosis.[1] Idiopathic pulmonary fibrosis (IPF), with an estimated prevalence of about 14–30 cases per 100 000 in the general population, is the canonical chronic fibrosing ILD associated with a median survival time of less than 5 years after diagnosis.[2] Other fibrosing ILDs are often associated with connective tissues diseases and may develop in ~18–32% of patients with ILDs, representing up to 20 patients per 100 000 people in Europe and

up to 28 patients per 100 000 in the USA, with the time from symptom onset to death estimated at 61–80 months.[3] Treatment options for progressive pulmonary fibrosis (PPF) are limited with only two approved drugs, nintedanib and, currently with a marketing authorisation only for IPF, pirfenidone, which only slow down fibrosis progression.[2] The unforeseeable progression of PPF is a clinical challenge. Despite increasing knowledge, the physiopathology of PPF remains misunderstood and finding new therapeutic targets and associated imaging predictive biomarkers are major clinical concerns to ameliorate cares towards personalised management. As there is currently no tool to predict disease progression in patients with PPF, even with treatment by nintedanib or pirfenidone due to the unpredictable interpersonal variability of efficiency, the identification of non-invasive biomarkers to promote early diagnosis and monitor fibrosis evolution is key to improve patients' outcome and therapy efficiency.

Macrophages with anti-inflammatory/profibrotic phenotype (M2), expressing CD206 on their surface, a C-type lectin mannose receptor, have been recently described as cells involved in the physiopathology of PPF, including IPF.[4] In fact, M2 macrophages, of which recruitment and polarisation towards the M2 phenotype are driven by M-CSF,[5] infiltrate fibrotic lungs[6] and produce high levels of profibrotic mediators such as transforming growth factor-β1 (TGF-β1), one of the main cytokines involved in fibrosis,[7] which induces myofibroblast activation and *in fine* fibrosis progression.[8] Interestingly, M2 macrophages have been used as therapeutic targets or imaging biomarkers through CD206 in various diseases such as rheumatoid arthritis (RA) or cancer.[9 10] Indeed, on one hand, M2 macrophage imaging can be achieved through technetium-99m labelled tilmanocept ($^{99m}$Tc-tilmanocept), a radiopharmaceutical suitable for in vivo single photon emission computed tomography (SPECT) imaging, with a high affinity for CD206.[11] On the other hand, the Janus-associated kinases JAK 1 and JAK 3 inhibitor tofacitinib has recently been shown to inhibit the polarisation of macrophages towards the M2 phenotype therefore reducing the pool of CD206$^+$-expressing macrophages and improving lung fibrosis in in vivo models of systemic sclerosis-associated and RA-associated interstitial lung disease (SSc-IILD and RA-ILD).[12 13] Importantly, the evaluation of the antifibrotic efficacy of tofacitinib is currently underway with a phase II (NCT05246293) and a phase IV (NCT04311567) clinical trial in patients with RA-ILD.

In this context, we hypothesised that CD206, through $^{99m}$Tc-tilmanocept in vivo SPECT imaging, could represent a non-invasive biomarker to monitor lung fibrosis progression and efficacy of existing and prospective antifibrotic therapies.

## MATERIAL AND METHODS

Detailed material and methods is available in online supplemental material.

### Animal experiments

Eight-week-old C57/Bl6 male mice (7 days of acclimatisation) received at D0 a single intratracheal injection of 2 mg/kg of bleomycin (BLM) (Santa Cruz Biotechnology, USA) or NaCl (controls) under anaesthesia (3% isoflurane). When indicated, animals were treated with nintedanib (Ofev, 60 mg/kg) or tofacitinib (Xeljanz, 30 mg/kg) by daily gavage during the fibrotic phase of BLM-induced lung fibrosis from D9 to D23. In this model, animals that did not react to BLM (measured by weight loss under 5% at day 5) are excluded from the study. In our experiments, only one mice was excluded. An automated randomisation method in Excel was used during the allocation to treatment groups and the order of animal treatments was performed randomly.

### Immunophenotyping of lung tissue cells

Cells obtained from lung tissue digestion were first resuspended in 100 µL phosphate-buffered saline (PBS) and stained on ice for 30 min with 1/1000th of BD Horizon Fixable Viability Stain 575V (565694, BD Biosciences). After washing step with PBS and centrifugation at 300×*g* for 5 min, pellet was then resuspended in Stain buffer (554656, BD Biosciences) with hamster anti-mouse CD16/32, clone 2.4G2 (554656, BD Biosciences) for 20 min in order to block Fc receptor-mediated binding of antibodies. These cells were then washed and incubated on ice for 30 min with fluorochrome-conjugated monoclonal antibodies (CD45, CD11b, CD11c, F4/80, Ly6g, SiglecF and CD206) diluted in BD Horizon Brilliant Stain Buffer (563794, BD Biosciences). After one more wash, cell fixation was performed with the BD Cytofix/Cytoperm fixation/permeabilization solution kit (554714, BD Biosciences) using the manufacturer's protocol. Cells were finally resuspended in 300 µL PBS before analysis on cytometer.

### Flow cytometry analysis

See online supplemental methods for details.

Post-acquisition analysis and compensation was performed with FlowJo V.10.7.2 (Treestar, USA) software. Data analysis was performed using supervised method. The expression of selected markers was presented as median fluorescence intensity (MFI). For gating control, fluorescence minus one (FMO) staining was used on cells where all antibodies except one were added to individual control tubes following the same protocol than antibodies staining.

### Single cell RNA sequencing of BLM-treated mice

See online supplemental methods for details.

Lung single cell suspensions were generated as previously described.[14] Clusters were annotated using canonical markers of endothelial, mesenchymal, epithelial and immune populations. Macrophages were extracted and subclustered using the same precomputed 80 PCs. UMAP was rerun on this subset. The original raw counts were finally log-normalised with NormalizeData for data exploration. Macrophage subpopulations were annotated according to their most differentially expressed genes described in Joshi *et al*.[5]

### In vivo imaging

Two pilot studies were performed on NaCl- and BLM-receiving mice at several stages by SPECT/CT with $^{99m}$Tc-tilmanocept (NaCl n=12, BLM D8 n=6, BLM D15 n=6, BLM D22 n=15). Mice were anaesthetised through isoflurane (1.5%) inhalation for intravenous injection (tail vein) of $^{99m}$Tc-tilmanocept (10 MBq, 235 µg/mouse) 1 hour before imaging. An additional group of mice received a concomitant injection of radiolabelled $^{99m}$Tc-tilmanocept with an excess (×100) of unlabelled tilmanocept (blocking, n=12). Mice were then maintained under anaesthesia (1.5% isoflurane) and placed on an imaging heated bed inside a NanoSPECT-CT (Mediso, Hungary). A CT scan of a lung-centred region was obtained (500 ms, 45 kV, 180 projections, pitch 1, binning 1:4) followed by SPECT acquisition with 90–120 s per projection frame, resulting in acquisition times of 45–60 min of the same region.

In other experiments, longitudinal imaging of lung fibrosis was performed on NaCl- (n=4) and BLM-receiving mice treated with vehicle (n=4), nintedanib (n=4) or tofacitinib (n=4) by successive SPECT/CT with $^{99m}$Tc-tilmanocept before BLM installation at D9, D16 and D23 following the same imaging protocol as described above.

For each experiments, after the last imaging, mice were sacrificed and lungs and blood were harvested for ex vivo quantification using a γ-counter (Wizard, PerkinElmer). Lungs were collected in 10% formalin for further histological analysis.

### Image analysis

All SPECT/CT fusion images were obtained using the VivoQuant software (Invicro, USA). Each image was visually interpreted and 3D regions of interest (3DROI) corresponding to the lungs were manually drawn for CT quantification and to determine their radioactivity content. Injected doses per animal were measured at the time of injection in MBq. Lung radioactivity content was expressed in MBq, converted to percentage of injected dose per gram of lung tissue (%ID/g). All images were decay-corrected for quantification. In addition, a semiautomatic segmentation of 3DROI was performed on CT scans as follows: normal lung density (−800 to −100 HU), corresponding to aerated lung areas, and high lung density (−100 to 300 HU), corresponding to non-aerated/fibrotic lung areas, as previously described.[15] This semiautomatic segmentation allowed the independent quantification of the radioactivity content of $^{99m}$Tc-tilmanocept in normal (aerated) and high (non-aerated) density lung tissue, respectively. All image analyses were performed in a blinded manner.

### Collagen quantification

For histochemical assay, the amount of collagen in paraffin-embedded tissue sections was quantified by staining with Picrosirius red as previously described.[16]

### Autoradiography

After deparaffination (xylene) and antigen unmasking (30 min in citrate buffer pH 6), sections from human biopsies from control or patients with IPF as well as mice receiving NaCl or BLM were saturated (bovine serum albumin (BSA) 8%) and incubated for 1 hour with $^{99m}$Tc-tilmanocept (1 MBq, 235 ng/slide). After four washes with coldDulbecco's phosphate buffered saline (DPBS), slides were exposed to phosphor imaging plates (Fuji imaging plates, Fujifilm). After 2–3 hours of exposure time, the imaging plates were scanned and the autoradiograms were obtained with a phosphor imaging system (GE, Amersham, Molecular Dynamics), and the images were analysed for count densities.

### Publicly available human datasets analysis

MRC1 expression was obtained via human gene expression profiles from patients with IPF collected from publicly available datasets (GSE110147, GSE68239 and GSE132607) on the Gene Expression Omnibus website. GSE110147 presents gene expression from fresh frozen lung samples obtained from the recipients' organs of 22 patients with IPF and 11 controls obtained from tissue flanking lung cancer resections. GSE68239 presents gene expression from lung tissues collected from patients with IPF undergoing lung transplantation. Samples were collected once from 'healthy looking' (non-fibrotic) regions and from fibrotic loci (n=10). Non-transplanted donor lung tissue showing no evidence of ILD served as healthy controls (n=8). GSE132607 presents gene expression data from the COMET-IPF which presents gene expression data from PBMC from non-progressor and progressor patients with IPF. In our analysis, progression was defined as a decrease in forced vital capacity (FVC) of 10% or greater or a decrease in diffusing capacity for carbon monoxide (DLCO) of 15% or greater as previously described.[17] Patients for whom no data were reported either at baseline or at 12 months were excluded.

### Statistical analysis

Comparison between two groups was performed using the Mann-Whitney non-parametric tests. Comparison between multiple groups has been performed using the Kruskal-Wallis non-parametric analysis of variance (ANOVA) tests. Correlations have been performed by linear regression using GraphPad Prism software. A $p<0.05$ was considered significant (*$p<0.05$, **$p<0.01$, ***$p<0.001$). Results are presented as median±IQR.

## RESULTS

### CD206 is a relevant target for in vivo imaging in experimental lung fibrosis and human IPF

Immunostaining of lung sections from NaCl- and BLM-receiving mice demonstrated that CD206 was upregulated both in fibrotic and non-fibrotic lung areas of BLM-receiving mice (figure 1A). CD206 expression strongly co-localised with CD68, a pan-macrophage marker, indicating that CD206 was mainly expressed by a subtype of macrophages in the fibrotic lung. These results were confirmed by anti-CD206 autoradiography using $^{99m}$Tc-tilmanocept (figure 1B). Areas with higher $^{99m}$Tc-tilmanocept signal corresponded to areas showing higher collagen content (figure 1B). In addition, the concomitant incubation with an excess of unlabelled-tilmanocept induced a competition with $^{99m}$Tc-tilmanocept and a significant decrease in autoradiographic signal in BLM-receiving mice demonstrating the specificity of the radiotracer (figure 1B).

Lung macrophages from whole lung extracts were further phenotyped by flow cytometry at several stages of BLM-induced lung fibrosis (online supplemental figure S1A). Clusterisation was performed in order to obtain 10 clusters of pulmonary cells identified according to the expression levels of phenotypic markers as previously described (online supplemental figure S1B, C).[18] Two macrophage populations were identified with a high CD206 expression (online supplemental figure S1D) including a tissue resident-alveolar macrophages (TR-AMs: CD45$^+$, CD11b$^-$, F4/80$^+$, CD11c$^{high}$, CD206$^{high}$, SiglecF$^+$) and a recruited population following BLM injury called monocyte-derived macrophages (Mo-AMs: CD45$^+$ CD11b$^+$ F4/80$^+$ CD11c$^+$ CD206$^{high}$ SiglecF$^{low}$). Among them, only Mo-AMs co-expressed CD206 and CD11b, suggesting an infiltrating population of circulating macrophages expressing CD206 (online supplemental figure S1D). As expected, Mo-AMs were not found in control mice while they arose upon BLM treatment at D8 and remained increased until D21 (online supplemental figure S1E).

Interestingly, while the MFI of CD206 in TR-AMs remained higher than in Mo-AMs throughout the experiment, BLM induced a switch in the dominant population as CD206$^+$ Mo-AMs became significantly more numerous than CD206$^+$ TR-AMs from D8 up to D22 (figure 1C).

Results were confirmed by performing single cell RNA sequencing (scRNAseq) on lung cells isolated from NaCl- or BLM-receiving mice at D14 and D28. Four populations were characterised (online supplemental figure S2A) based on their transcriptomic profile (online supplemental figure S2B) as

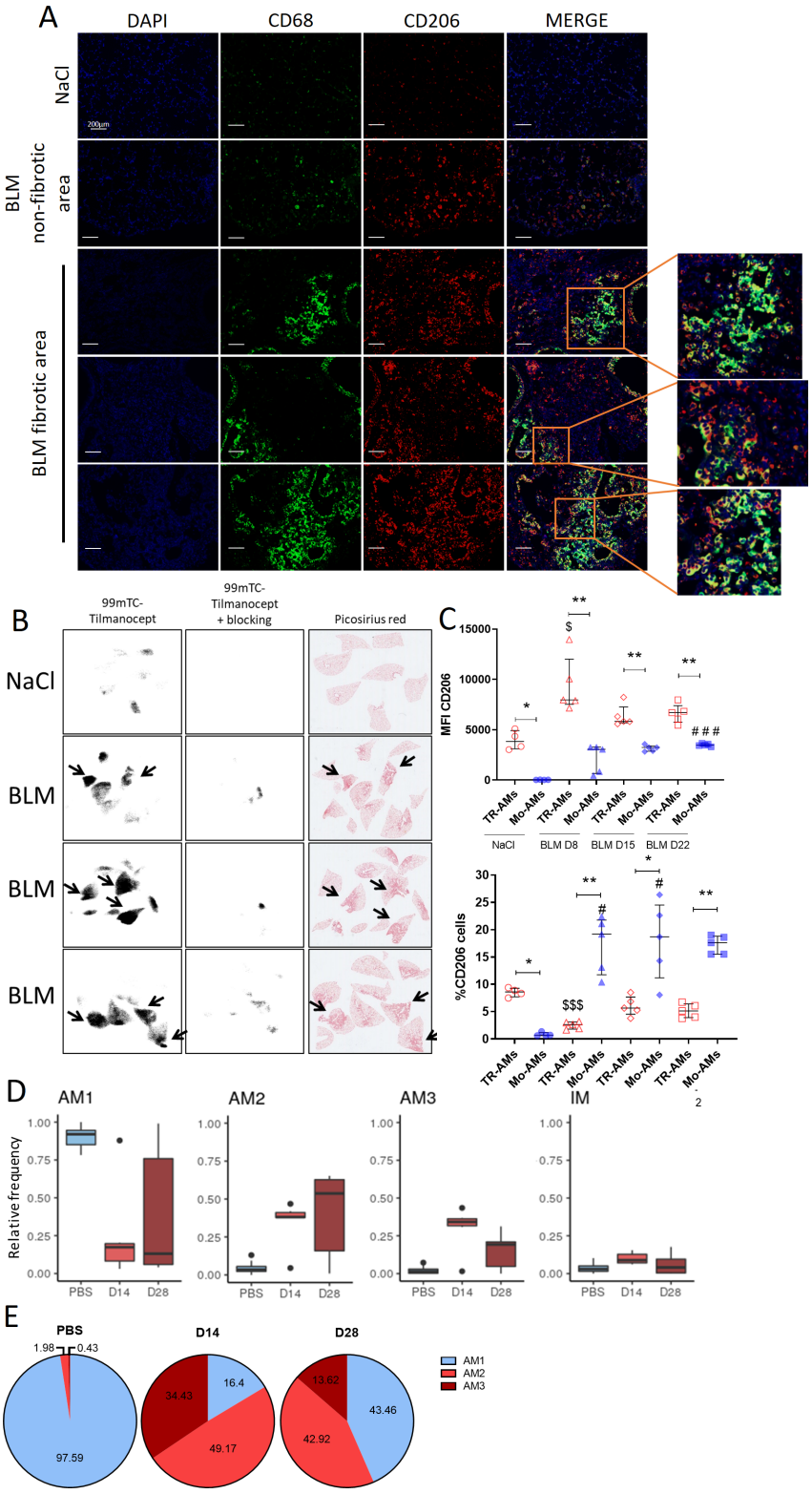


**Figure 1** CD206 is a relevant target in lung fibrosis. (A) Representative immunohistochemistry (IHC) staining of CD206 (red) and CD68 (green) on lung sections from mice receiving NaCl or bleomycin (BLM, D21). Scale bar=200 µm. (B) $^{99m}$Tc-tilmanocept autoradiography images and Picosirius red images on lung sections from mice receiving NaCl or BLM (D21). (C) CD206 expression were quantified using median fluorescence intensity (MFI) or expressed in percentage of cells expressing CD206 in TR-AMs and Mo-AMs cells. Results are presented as median±IQR, NaCl n=4, BLM D8 n=5, BLM D15 n=5, BLM D22 n=5. Star (*) is a representative of comparison of Mo-AMs with TR-AMs analysed by t-test Mann-Whitney. Dollar ($) is a representative of statistical comparison of each TR-AMs group with TR-AMs NaCl, hash (#) is a representative of statistical comparison of each Mo-AMs group with Mo-AMs NaCl. The difference between groups was compared using Kruskal-Wallis non-parametric analysis of variance (ANOVA), *($^{/\#}$)p<0.05, **($)p<0.01, ***($^{\$\$\$/\#\#\#}$)p<0.001. (D) Frequency of each macrophage subpopulation relative to all other macrophages by scRNAseq, calculated for individual mice treated with phosphate-buffered saline (PBS, n=18) or BLM (n=6 for each time point). (E) CD206 gene (*Mrc1*) expression relative to the proportion of AM1, AM2 and AM3 cells at the basal level (PBS) or after 14 or 28 days post-BLM.

previously described,[5] corresponding to interstitial macrophages and three populations of alveolar macrophages noted AM1, AM2 and AM3. AM1 were characterised by a high expression of *Siglecf* and a low expression of *Itgam* corresponding to TR-AMs, while AM3 showed an opposite expression profile (*Siglecf* $^{low}$, *Itgam*$^{high}$) corresponding to Mo-AMs (online supplemental figure S2C). AM2 showed an intermediate expression profile with the loss of *Siglecf* expression (online supplemental figure S2C). We observed a significant drop of the AM1 population upon BLM administration along with an influx of AM2 and AM3 mainly at the time of progressive BLM-induced lung fibrosis (D14, figure 1D), whereas IMs remained unchanged. Interestingly, in NaCl-receiving mice, CD206 gene (*Mrc1*) expression mainly came from AM1 (TR-AMs) cells as they represent the large majority of physiological AMs, while on BLM (D14 and D28), *Mrc1* expression was mainly driven by AM2 and AM3 (Mo-AMs, figure 1E).

In human, immunostaining and autoradiographic signal of $^{99m}$Tc-tilmanocept of lung biopsies from patients with IPF and controls demonstrated that CD68$^+$/CD206$^+$ macrophages were upregulated in IPF (figure 2A,B) but not in control lungs. Further, publicly available transcriptomic datasets on lung tissue from patients with IPF and controls demonstrated that *Mrc1* (CD206 gene) was upregulated in IPF lungs, suggesting the influx of CD206$^+$ macrophages in the lung of patients with IPF (figure 2C). Interestingly, this upregulation of *Mrc1* was found both in fibrotic and non-fibrotic areas of IPF tissues (figure 2D). *Mrc1* was upregulated in patients with IPF with a progressive disease compared with patients with IPF who did not show progression over a year (figure 2E), demonstrating the potential interest of CD206 as a marker of active fibrosis in patients with IPF.

### SPECT in vivo imaging can detect the increase in CD206 in BLM-induced lung fibrosis

NaCl- and BLM-receiving mice underwent SPECT/CT imaging with $^{99m}$Tc-tilmanocept at several stages of experimental fibrosis (figure 3A). The $^{99m}$Tc-tilmanocept lung uptake was significantly increased in BLM-treated mice at D8, D15 and D22 compared with NaCl-receiving mice (D22) (figure 3B,C, online supplemental table S1 and figure S3A). The concomitant administration of an excess of unlabelled-tilmanocept induced a competition with $^{99m}$Tc-tilmanocept and a significant decrease in SPECT signal in fibrotic mice demonstrating the specificity of the radiotracer (figure 3B,C). The global biodistribution of $^{99m}$Tc-tilmanocept demonstrated that major uptake was found in elimination organs such as the liver and the bladder (online supplemental figure S3B, C). Blocking experiments only induced a decrease in lung uptake without affecting other organs further demonstrating the specificity of $^{99m}$Tc-tilmanocept lung uptake in BLM-receiving mice (online supplemental figure S3B, C).

In parallel, the lung CT of BLM-receiving mice showed an increase in fibrotic consolidations (corresponding to mean lung density (MLD)) compared with control mice at D8, D15 and D22 (figure 3D and online supplemental table S2). Similar to immunostainings (figure 1A), $^{99m}$Tc-tilmanocept SPECT signal was increased in both aerated and non-aerated lung areas in BLM-receiving mice compared with the control mice (online supplemental figure S3D). Interestingly, $^{99m}$Tc-tilmanocept lung uptake on SPECT significantly positively correlated with MLD measured on CT (figure 3E).

### In vivo imaging of CD206 is a useful tool to monitor nintedanib efficacy

NaCl- and BLM-receiving mice treated or not with nintedanib underwent longitudinal imaging with $^{99m}$Tc-tilmanocept successively at D0, D9, D16 and D23 (figure 4A). Lung uptake of $^{99m}$Tc-tilmanocept increased at early stage (D9) in BLM-receiving mice and remained higher compared with control up to D23 (figure 4B, online supplemental table S3 and figure S4A). In BLM-receiving mice, nintedanib dramatically decreased $^{99m}$Tc-tilmanocept lung uptake at D16 and D23 (figure 4B and online supplemental figure S4A). Similarly, MLD measured on CT and collagen quantification on lung sections significantly increased from D9 to D23 in BLM-receiving mice and were decreased by nintedanib (figure 4C,D and online supplemental table S4). Interestingly, $^{99m}$Tc-tilmanocept uptake at D9 negatively correlated with the variation of MLD ($\Delta CT^{D9\text{-}D23}$) in nintedanib-receiving mice, suggesting that lungs with higher $^{99m}$Tc-tilmanocept uptake at D9 were those in which nintedanib showed the best efficacy (figure 4E). Furthermore, nintedanib significantly reduced the percentage of CD206$^+$ Mo-AMs induced on BLM without affecting CD206$^+$ TR-AMs (figure 4F and online supplemental figure S4B).

In vitro, nintedanib induced a dose-dependent inhibition of interleukin (IL)-4-induced M2 polarisation associated with a decrease in CD206$^+$ macrophage (online supplemental figure S5A) but did not decrease the phosphorylation of CSFR1, AKT and ERK (online supplemental figure S5B). Further, nintedanib inhibited the ability of conditioned media from macrophages treated with IL-4 to promote myofibroblast differentiation as shown by the reduced expression of *Acta2*, *Col1A*, *Col3A1* and *Fn* genes in CCD-19Lu human fibroblasts (online supplemental figure S5C). On the contrary, nintedanib did not directly inhibit CD206 expression nor the production of profibrotic mediators in already differentiated M2 macrophages (online supplemental figure S5D, E). These results suggesting that nintedanib did not play a role in M2 macrophages repolarisation were confirmed by immunoblotting demonstrated that nintedanib did not hamper phosphorylation of STAT3, NFκB, JAK1 and JAK3 in already differentiated M2 macrophages (online supplemental figure S5F).

### In vivo imaging of CD206 is a useful tool to monitor tofacitinib antifibrotic efficacy

A similar imaging protocol than with nintedanib was used (figure 4A). Lung uptake of $^{99m}$Tc-tilmanocept increased at early stage (D9) in BLM-receiving mice and remained higher compared with the control up to D23 (figure 5A and online supplemental figure S6A). In BLM-receiving mice, tofacitinib dramatically decreased $^{99m}$Tc-tilmanocept lung uptake at D16 and D23 (figure 5A, (online supplemental table S5 and figure S6A). In parallel, MLD measured on CT and collagen quantification on lung sections significantly increased from D16 to D23 in BLM-receiving mice and these effects were prevented by tofacitinib (figure 5B,C and online supplemental table S6).

As observed for nintedanib, $^{99m}$Tc-tilmanocept uptake at D9 positively correlated with the variation of MLD ($\Delta CT^{D9\text{-}D23}$) in BLM-receiving mice (figure 5D) while negatively correlated with the variation of MLD ($\Delta CT^{D9\text{-}D23}$) in tofacitinib-receiving mice (figure 5E). These findings suggest that early $^{99m}$Tc-tilmanocept lung uptake could be predictive of lung fibrosis progression and tofacitinib efficacy. In parallel, tofacitinib significantly reduced the percentage of CD206$^+$ Mo-AMs

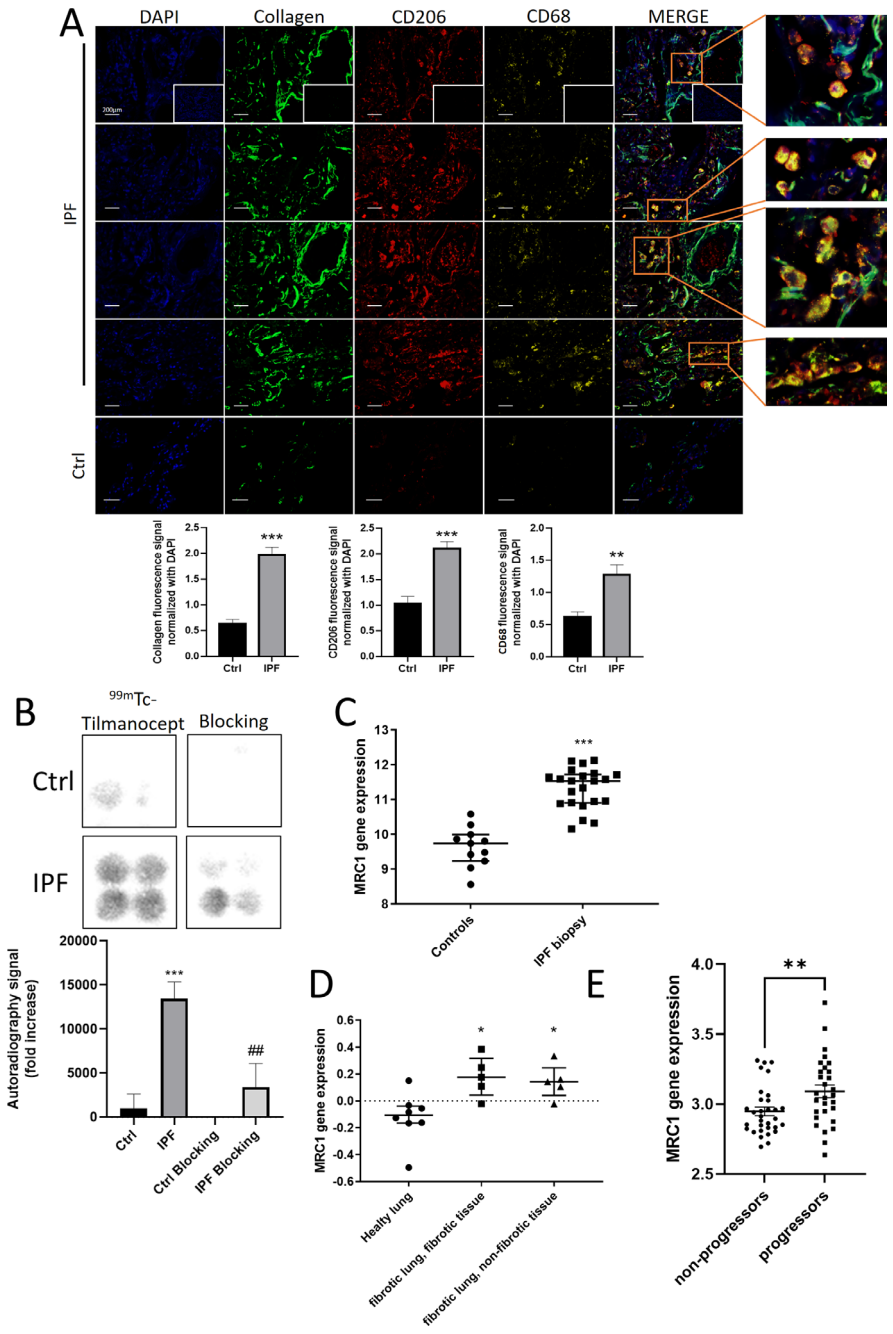


**Figure 2** CD206 is a relevant target in human idiopathic pulmonary fibrosis (IPF). (A) Representative immunohistochemistry (IHC) staining and quantification of collagen (green), CD206 (red) and CD68 (yellow) on human lung biopsies from control and patients with IPF (scale bar=200 µm). White boxes in the top row are negative controls. Results are presented as median±IQR, n=8 for both groups. The difference between groups was compared using Mann-Whitney non-parametric t-test, **p<0.01, ***p<0.001. (B) Autoradiography images and quantification of $^{99m}$Tc-tilmanocept on human lung biopsies from controls and patients with IPF. Results are presented as median±IQR, n=8 for both groups. Star (*) is a representative of comparison of each group with the NaCl group and hash (#) is a representative of statistical comparison of blocking group with the IPF group. The difference between groups was compared using Kruskal-Wallis non-parametric analysis of variance (ANOVA). $^{\#\#}$p<0.01, ***p<0.001. (C) Analysis of *Mrc1* gene expression of publicly available microarray data (accession number GSE110147) from lung samples from 22 patients with IPF undergoing lung transplantation and 11 normal lung tissues flanking lung cancer resections. Results are presented as median±IQR. The difference between groups was compared using Mann-Whitney non-parametric t-test. ***p<0.001. (D) Analysis of *Mrc1* gene expression of publicly available microarray data (accession number GSE68239). Lung tissues were collected from patients with IPF undergoing lung transplantation. Non-transplanted donor lung tissue showing no evidence of interstitial lung disease served as healthy controls. From each of patients with IPF, samples were collected once from 'healthy looking' (non-fibrotic) regions and from fibrotic loci. Results are presented as median±IQR, n=5 for controls and n=5 for non-fibrotic and fibrotic IPF tissue. The difference between groups was compared using Kruskal-Wallis non-parametric ANOVA. *p<0.05. (E) Analysis of *Mrc1* gene expression of publicly available microarray data (accession number GSE132607) from PBMC from patients with IPF who underwent pulmonary function tests over at least two time points. Patients experiencing a decrease in forced vital capacity (FVC) of 10% or greater or a decrease in diffusing capacity for carbon monoxide (DLCO) of 15% or greater over 12 months were considered as progressors. Results are presented as mean±SEM, n=32 for non-progressors and n=29 for progressors, *p<0.01, unpaired t-test.

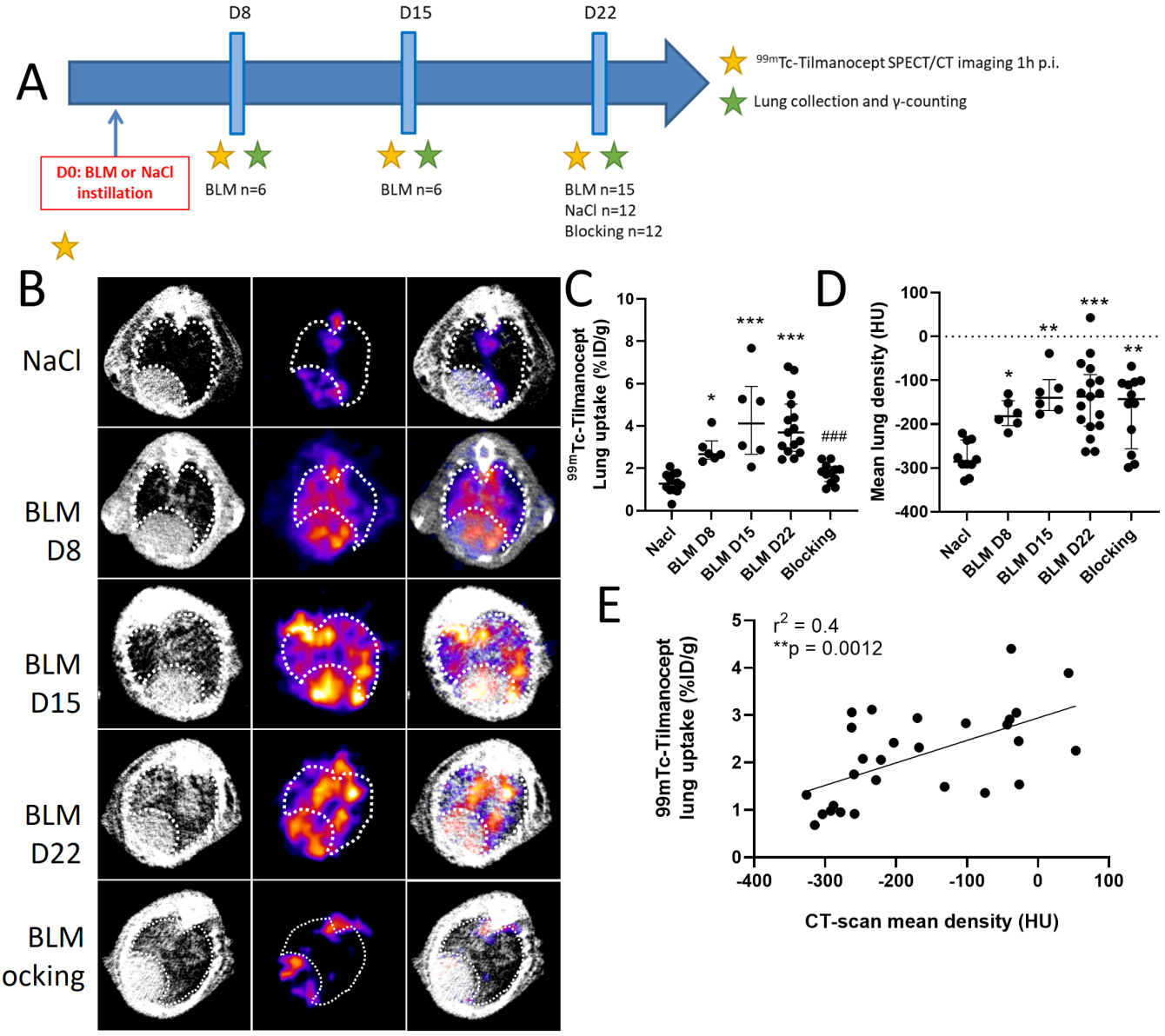


**Figure 3** $^{99m}$Tc-tilmanocept is able to detect advanced bleomycin (BLM)-induced lung fibrosis. (A) Schematic representation of the design of the study of $^{99m}$Tc-tilmanocept imaging in NaCl- and BLM-receiving mice at several stage of experimental fibrosis. (B) Representative lung single photon emission computed tomography/CT (SPECT/CT) images with $^{99m}$Tc-tilmanocept of NaCl- and BLM-receiving mice at D8, D15 and D22 (the lung region is represented by the dotted circle). (C) Graph represents the $^{99m}$Tc-tilmanocept lung uptake in %ID/g of NaCl- and BLM-receiving mice at D8, D15 and D22. Results are presented as median±IQR, NaCl n=12, BLM D8 n=6, BLM D15 n=6, BLM D22 n=15. Star (*) is a representative of comparison of each group with the NaCl group and hash (#) is a representative of statistical comparison of blocking group with the BLM D22 group. The difference between groups was compared using Kruskal-Wallis non-parametric analysis of variance (ANOVA), *p<0.05, ***(###)p<0.001. (D) Graph represents the mean lung density quantified on CT images of NaCl- and BLM-receiving mice at D8, D15 and D22. Results are presented as median±IQR, NaCl n=12, BLM D8 n=6, BLM D15 n=6, BLM D22 n=15. The difference between groups was compared using Kruskal-Wallis non-parametric ANOVA. *p<0.05, **p<0.01, ***p<0.001. (E) Correlation between mean lung densities (HU) measured on CT images and $^{99m}$Tc-tilmanocept lung uptake (%ID/g) of the corresponding lungs measured on SPECT/CT.

induced on BLM without affecting CD206$^+$ TR-AMs (online supplemental figure S6A).

In vitro, tofacitinib significantly inhibited IL4-induced CD206$^+$ macrophage polarisation in a dose-dependent manner (online supplemental figure S6C) and decreased the phosphorylation of CSFR1, AKT and ERK (online supplemental figure S5B). Further, tofacitinib inhibited the ability of conditioned media from macrophages treated with IL-4 to promote myofibroblast differentiation as shown by reduced expression of *Acta2*, *Col1A*, *Col3A1* and *Fn* genes in CCD-19Lu human fibroblasts (online supplemental figure S5C). Similar to nintedanib, tofacitinib did not induce a direct inhibition of CD206 expression (online supplemental figure S6D) and did not inhibit the production of profibrotic mediators in already differentiated M2 macrophages (online supplemental figure S5E). These results suggesting that

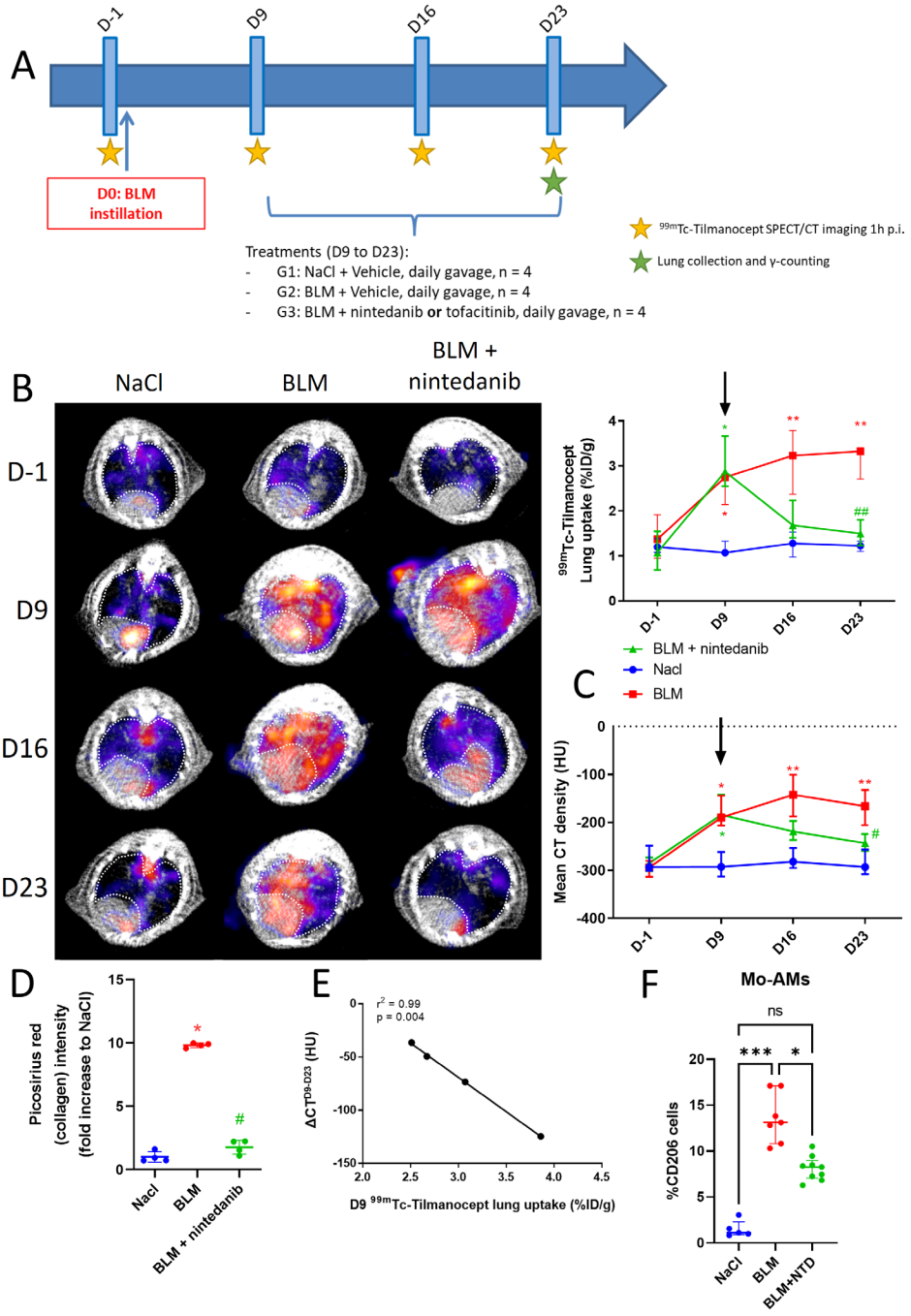


**Figure 4** In vivo imaging of CD206 is a useful tool to monitor nintedanib efficacy. (A) Schematic representation of the design of the longitudinal study of $^{99m}$Tc-tilmanocept imaging with nintedanib or tofacitinib treatments. (B) Representative $^{99m}$Tc-tilmanocept single photon emission computed tomography/CT (SPECT/CT) images of NaCl- and bleomycin (BLM)-receiving mice treated or not with nintedanib at D-1, D9, D16 and D23 (the lung region is represented by the dotted circle). Graph represents evolution of $^{99m}$Tc-tilmanocept lung uptake (%ID/g) at all time points. Results are presented as median±IQR, n=4 for all groups. Star (*) is a representative of statistical comparison between time points for each groups and hash (#) is a representative of statistical comparison between the groups at each time points. The difference between groups was compared using Kruskal-Wallis non-parametric analysis of variance (ANOVA), *p<0.05, **(##)p<0.01. Black arrow represents the start of treatments. (C) Graph represents evolution of mean lung densities (mean CT density) of NaCl- and BLM-receiving mice treated or not with nintedanib at D-1, D9, D16 and D23. Results are presented as median±IQR, n=4 for all groups. Star (*) is a representative of statistical comparison between time points for each group and hash (#) is a representative of statistical comparison between the groups at each time point. The difference between groups was compared using Kruskal-Wallis non-parametric ANOVA, *(#)p<0.05, **p<0.01. Black arrow represents the start of treatments. (D) Graph represents the intensity of Picrosirius red staining on lung section from of NaCl- and BLM-receiving mice treated or not with nintedanib at D23. Results are presented as median±IQR, n=4 for all groups. Star (*) is a representative of comparison of each group with the NaCl group and hash (#) is a representative of statistical comparison of the BLM and BLM+nintedanib groups. The difference between groups was compared using Kruskal-Wallis non-parametric ANOVA, *(#)p<0.05. (E) Correlation of $^{99m}$Tc-tilmanocept lung uptake at D9 and variation of CT quantification between D9 and D23 in BLM+nintedanib-treated mice. (F) CD206 expression at D23 was expressed in percentage of cells expressing CD206 Mo-AMs cells. Results are presented as median±IQR, NaCl n=5, BLM n=7, BLM+NTD n=9. The difference between groups was compared using Kruskal-Wallis non-parametric ANOVA, *p<0.05, ***p<0.001.

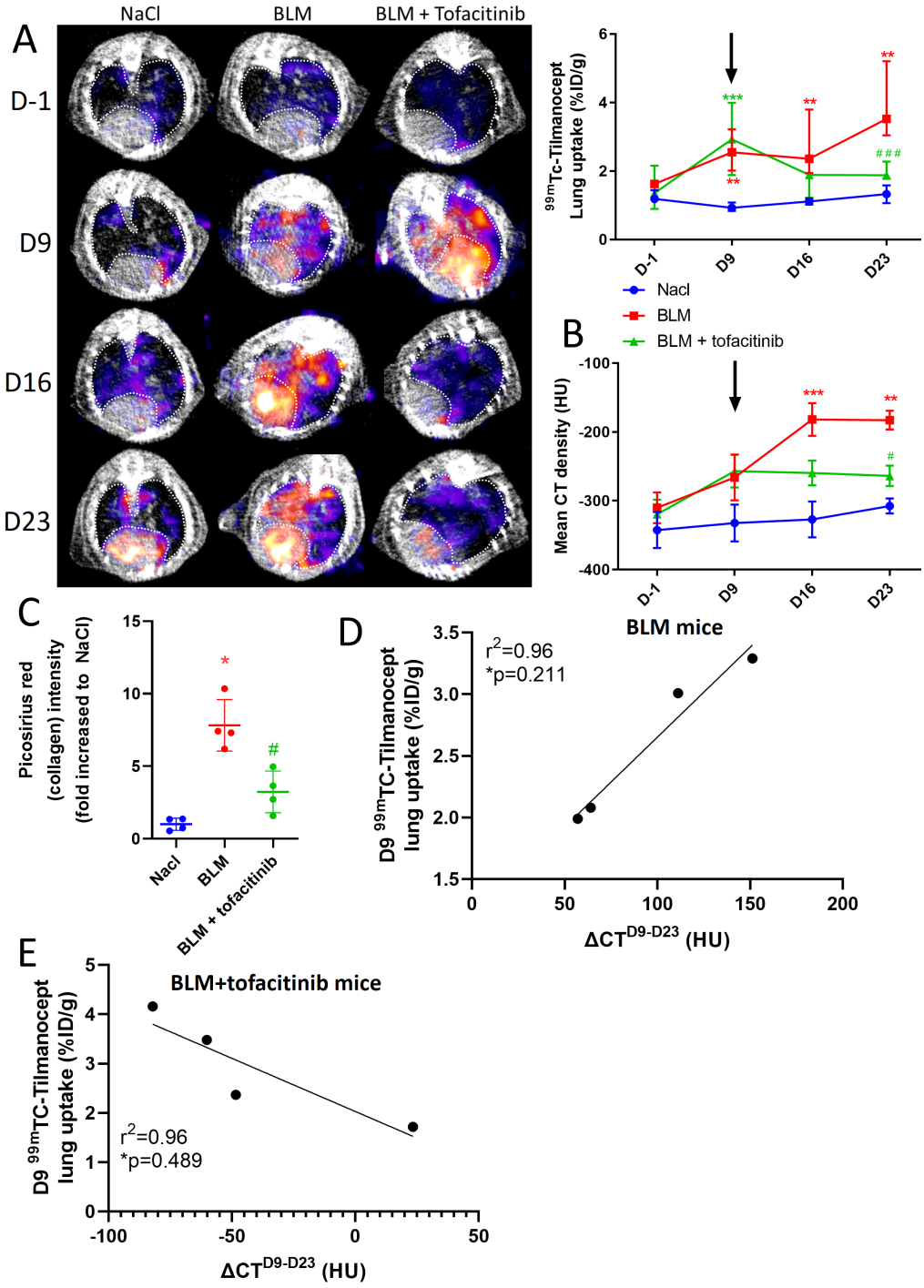


**Figure 5** In vivo imaging of CD206 is a useful tool to monitor tofacitinib efficacy. (A) Representative $^{99m}$Tc-tilmanocept single photon emission computed tomography/CT (SPECT/CT) images of NaCl- and bleomycin (BLM)-receiving mice treated or not with tofacitinib at D-1, D9, D16 and D23 (the lung region is represented by the dotted circle). Graph represents evolution of $^{99m}$Tc-tilmanocept lung uptake (%ID/g) at all time points. Results are presented as median±IQR, n=4 for all groups. Star (*) is a representative of statistical comparison between time points for each group and hash (#) is a representative of statistical comparison between the groups at each time points. The difference between groups was compared using Kruskal-Wallis non-parametric analysis of variance (ANOVA), **p<0.01, ***(###)p<0.001. Black arrow represents the start of treatments. (B) Graph represents evolution of mean lung densities of NaCl- and BLM-receiving mice treated or not with tofacitinib at D-1, D9, D16 and D23. Results are presented as median±IQR, n=4 for all groups. Star (*) is a representative of statistical comparison between time points for each group and hash (#) is a representative of statistical comparison between the groups at each time point. The difference between groups was compared using Kruskal-Wallis non-parametric ANOVA, #p<0.05, **p<0.01, ***p<0.001. Black arrow represents the start of treatments. (C) Graph represents the intensity of Picrosirius red staining on lung section from NaCl- and BLM-receiving mice treated or not with tofacitinib at D23. Results are presented as median±IQR, n=4 for all groups. Star (*) is a representative of comparison of each group with the NaCl group and hash (#) is a representative of statistical comparison of BLM and BLM+tofacitinib groups. The difference between groups was compared using Kruskal-Wallis non-parametric ANOVA, *(#)p<0.05. (D) Correlation of $^{99m}$Tc-tilmanocept lung uptake at D9 and variation of CT quantification between D9 and D23 in BLM-treated mice. (E) Correlation of $^{99m}$Tc-tilmanocept lung uptake at D9 and variation of CT quantification between D9 and D23 in BLM+tofacitinib-treated mice.

tofacitinib did not play a role in M2 macrophage repolarisation which were confirmed by immunoblotting demonstrated that tofacitinib did not hamper the phosphorylation of STAT3, NFκB, JAK1 and JAK3 in already differentiated M2 macrophages (online supplemental figure S5F).

## DISCUSSION

Macrophages have a high plasticity and can acquire several phenotypes depending on the microenvironment. In fibrotic lungs, anti-inflammatory/profibrotic (M2) macrophages produce high levels of profibrotic mediators such as TGF-β1.[7 19 20] Here, we demonstrate in our experimental preclinical models that CD206$^+$ macrophages are upregulated at the early stages of lung fibrosis development and remain present at high levels up to later stages. Among macrophages in the lungs, AMs have been clearly identified as the population responsible for the resolution of inflammation and tissue repair.[21] We described, as Misharin *et al* in their study, a heterogeneity of AMs in the lungs with two main populations, tissue resident AMs (TR-AMs) and monocyte-derived recruited AMs (Mo-AMs) appearing during BLM-induced lung fibrosis in mice.[18 22] The deletion of Mo-AMs after their recruitment to the lung is able to prevent fibrosis, whereas the deletion of TR-AMs had no effect on fibrosis severity, suggesting that progression of lung fibrosis is mainly driven by Mo-AMs.[22] Our study highlights the kinetic of Mo-AMs polarisation/recruitment in the lungs after BLM challenge. These findings are in accordance with previous studies demonstrating that BLM induces apoptosis of TR-AMs[23] which may be replaced by a major increase in Mo-AMs after BLM-induced inflammation.[4 5 24] Our single cell approach further confirms the emergence of a Mo-AMs population (AM2/AM3) in fibrotic conditions with an enriched expression of fibrosis-related genes (online supplemental figure S2). In line with their profibrotic properties, Mo-AMs represent the main macrophage population present in the lungs under fibrotic conditions and are therefore responsible for the increase in CD206 expression upon BLM in mice. Consequently, these findings highlight CD206 as a potent biomarker to monitor fibrosis progression and activity.

The main clinical challenge in PPF is the unpredictable evolution of lung fibrosis and also the impossible monitoring of the efficacy of antifibrotic therapies. Our group and others recently demonstrated that longitudinal CT scan in preclinical BLM-induced lung fibrosis was a reliable tool to monitor the severity and progression of lung fibrotic areas by determining MLD.[15] Here, we demonstrate that in vivo longitudinal imaging of CD206$^+$ cells is able to specifically and accurately detect lung fibrosis severity and progression in correlation with CT imaging. Importantly, we demonstrate in fibrotic lungs that $^{99m}$Tc-tilmanocept lung uptake is also increased in seemingly normal lung areas in CT scans (aerated areas) and CD206$^+$ macrophages are found in histologically 'normal' areas suggesting that CD206 imaging may help to detect early fibrotic lesions not yet visible on CT scans. Interestingly $^{99m}$Tc-tilmanocept imaging did not show a high background in the lung of untreated mice although we identified by flow cytometry a TR-AMs population expressing high basal levels of CD206 in their lungs. In addition, the signal-to-background ratio in $^{99m}$Tc-tilmanocept SPECT images was sufficient for an accurate quantification of fibrosis in BLM-treated mice compared with controls. Even if TR-AMs show a high expression of CD206, their proportion in the untreated lung remains likely too low to generate a residual lung uptake. Nevertheless, $^{99m}$Tc-tilmanocept imaging need to be further investigated in humans in order to determine whether the threshold of detection of CD206 between healthy individuals and patients with PPF is relevant for the use of $^{99m}$Tc-tilmanocept as a diagnostic/follow-up imaging tool in this disease. In addition, the global biodistribution of $^{99m}$Tc-tilmanocept highlighted a slight increase in the liver, spleen and blood upon BLM which could be explained by an increase in soluble CD206 in the serum, shed from activated M2-macrophages, that has been reported during fibrosis and has been correlated with mortality in patients with IPF.[25] The complete investigation of soluble CD206 may require more in-depth attention in future preclinical and clinical studies. Further, our data demonstrate that *CD206* gene expression in human is increased in the lungs of non-progressor versus progressor patients with IPF. Human gene expression analysis was performed on a publicly available dataset (GSE132607) and progression of IPF was define as a decrease in FVC of 10% or greater or a decrease in DLCO of 15% or greater as described in the COMET study[17] and according to ERICE recommendations.[26] One limitation of this analysis resides in the lack of clinical data on the patients that did not allow us to ensure that the drop in DLCO was not due to a comorbidity other than IPF. Nevertheless, these clinical data are another evidence supporting CD206 as a biomarker which may improve the management of patients with IPF.

Our study confirms in vitro and in vivo the results of Bellamri *et al,* which showed that nintedanib considerably altered human macrophages phenotype towards a reduction of M2 markers including CD206.[27] Nintedanib induced a rapid decrease in CD206$^+$ Mo-AMs in the lungs with minimal impact on CD206 expression itself, suggesting that nintedanib may be, at least in part, driven by a role on M2 polarisation. This hypothesis is supported by previous reports.[27] However, the clinical relevance of the effect of nintedanib on M2 polarisation should be taken with caution since nintedanib inhibits macrophage functions in vitro at higher concentrations than those measured in patients.[28] Most importantly, our data suggest that $^{99m}$Tc-tilmanocept imaging may be a useful tool to predict nintedanib efficacy. Early high levels of $^{99m}$Tc-tilmanocept uptake in the lungs correlated with a high efficacy of nintedanib in animals. These findings are of primary interest as prediction of antifibrotic drugs' efficacy currently remains a major clinical issue.

Therapeutic strategies targeting CD206$^+$ macrophages in lung fibrosis have recently been shown to be efficient in preventing fibrosis progression.[29 30] It has been demonstrated that the CD206-specific blocking peptide RP-832c significantly reduced BLM-induced fibrosis with decreased CD206, TGF-β1 and α-SMA expression in mice. Interestingly, RP-832c did not induce any change in TR-AM markers suggesting that CD206 inhibition and subsequent fibrosis prevention was mainly due to an action on Mo-AMs.[30] In addition, Wang *et al* demonstrated that microcystin-LR, a cyclic peptide produced by cyanobacteria, was able to ameliorate experimental lung fibrosis via the inhibition of CD206$^+$ M2-like macrophage polarisation.[29] In accordance with these findings, we demonstrate here that tofacitinib, a JAK inhibitor known to be able to inhibit M2 macrophage polarisation,[13 31] induced a loss of CD206$^+$ cell population in the lung associated with a reduction of lung fibrosis, similarly to nintedanib. In our study, tofacitinib and nintedanib did not directly impact CD206 expression at early stages of fibrosis progression, suggesting that the decrease in CD206$^+$ cell population may be either the consequence of a lower recruitment of Mo-AMs or an inhibition of M2 macrophage polarisation rather than a direct inhibition of CD206 expression or the promotion of M2 macrophage

repolarisation. Based on our findings, reduction of CD206$^{+}$ cell population appears as a novel therapeutic strategy for lung fibrosis. However, similarly to nintedanib, these results may need to be taken carefully as tofacitinib doses used in preclinical models are twofold to threefold higher than corresponding doses in humans.[32] Nevertheless, tofacitinib is under investigation in scleroderma and approved for the treatment of RA,[33] two pathologies with a significant proportion of patients who ultimately develop progressive lung fibrosis.[34 35] A post hoc analysis of 21 clinical trials showed a lower incidence rate of progressive lung fibrosis in patients with RA under tofacitinib treatment compared with placebo,[36] and several case reports demonstrated a beneficial effect of tofacitinib on pre-existing progressive lung fibrosis in patients with RA.[37 38] Similarly, Chen *et al* demonstrated that tofacitinib ameliorated survival, lung function parameters and findings on high-resolution computed tomography (HRCT) in patients with PPF associated with amyopathic dermatomyositis.[39] In addition, the ongoing clinical trials PULMORA (NCT04311567) and RAILDTo (NCT05246293), which aim at demonstrating the efficacy of tofacitinib to reduce lung fibrosis and improve pulmonary function in patients with RA-ILD, further support the potential value of this type of therapy in the treatment of progressive fibrosis including IPF.

While our preclinical results are certainly promising, their relevance for human PPF needs further investigation. Indeed, BLM-induced fibrosis may show some important limitations for clinical translation regarding the study of M2 macrophages. For instance, in our study BLM induces a massive recruitment of Mo-AMs in the lungs at D9, which may not be occurring in patients who usually come to the clinic at late stages of the disease. In addition, despite the fact that in vivo imaging allows longitudinal evaluation of CD206 expression in animals, the small sample size in our in vivo experiments may be a limitation of our study and warrant further in vivo confirmation. Nevertheless, we report here that CD206 is upregulated in the biopsies of patients with IPF and that $^{99m}$Tc-Tilmanocept is able to detect this upregulation ex vivo. This constitutes a first step towards the validation of this radiotracer for further investigations in humans. In addition, our data from human gene expression clearly demonstrate that CD206 is a relevant theranostic target in PPF.

**Author affiliations**
[1]HSP-pathies Team, INSERM U1231 CTM Labex LIPSTIC and Label of Excellence from la Ligue National Contre le Cancer, Dijon, France
[2]Pneumology and Respiratory Intensive Care, CHU Dijon, Dijon, France
[3]Reference Center for Rare Pulmonary Diseases, OrphaLung Network, RespiFil, CHU Dijon Bourgogne, Dijon, France, Valbonne, France
[4]Faculty of Medicine and Pharmacy, University of Burgundy, Dijon, France, Dijon, France
[5]Université Côte d'Azur, IPMC, UMR CNRS 7275 Inserm 1323, IHU RespiERA, Valbonne, France
[6]Team IMATHERA, Centre Georges François Leclerc, Dijon, France
[7]Institut de Chimie Moléculaire de l'Université de Bourgogne, UMR 6302, CNRS, Université de Bourgogne, Dijon, France
[8]FHU-OncoAge, CNRS, IPMC, Université Côte d'Azur, Valbonne, France
[9]Department of Medicine, Pathology, and Molecular Medicine, McMaster University, Dijon, Ontario, Canada

**X** Leo Biziorek @LBiziorek

**Acknowledgements** Flow cytometry/microscopy experiments were performed at the ImaFlow core facility (Biologie Santé Dijon BioSanD US58, 21079, Dijon, France) and supported by Burgundy Regional Council. We would like to thank Camille Drouet, Valérie Bordat and Mélanie Guillemin for their technical help. This work was performed within Pharm'image, a regional centre of excellence in pharmacoimaging. The authors also thank the technical support of the UCA GenomiX platform of the University Côte d'Azur and the staffs from the animal care facilities institutions at Sophia Antipolis (IPMC Animal Care Facility).

**Contributors** Conceptualisation: LP, GB, CG, BC, BM, MRJK, PB, OB, FG, P-SB. Methodology: LP, GB, LB, MT, JT, AMMD, LD, N Pernet, VG, AB, MM, N Pottier, GS, P-SB. Investigation: LP, GB, LB, MT, AMMD, JT, LD, N Pernet, VG, AB, MM, N Pottier, GS, OB, P-SB. Funding acquisition: PB, OB, P-SB. Supervision: CG, KA, BC, BM, PB, OB, FG, P-SB. Writing—original draft: LP, GB, FG, P-SB. Guarantor: PB. Writing—review and editing: All authors.

**Funding** This project was supported by Agence National de la Recherche (HYMAGE-IPF: ANR-20-CE17-0005, SMART-PROGRESS: ANR-21-CE17-0065 and ANR-PRCI-18-CE92-0009-01). JT and LB are funded by La Fondation du Souffle et le Fonds de Recherche en Santé Respiratoire FR-2019. OB has received funding from the European Respiratory Society and the European Union's H2020 research and innovation programme under the Marie Sklodowska-Curie (grant agreement No. 713406). OB is supported by the French "Investissements d'Avenir" programme, project ISITE-BFC (ANR-15-IDEX-0003). We also thank for their financial support the Canceropôle PACA, the Ruban Rose Foundation, the Institut National du Cancer (INCa PLBIO-22-093), la Ligue contre le cancer (CG and PB have the label d'excellence from la Ligue National contre le Cancer), the "Conseil Regional de Bourgogne" and the FEDER. Support was also provided by the French Government through the French National Research Agency (ANR) under the programme "Investissements d'Avenir" (ANR-10-EQPX-05-01/IMAPPI Equipex, ANR-11-LABX-0021 LipSTIC and ANR-11-LABX-0051 GR-Ex).

**Competing interests** None declared.

**Patient consent for publication** Not applicable.

**Ethics approval** Lung tissue samples (n = 8) were obtained by open lung biopsy with patient consent in compliance with the Research Ethics Board of St Joseph's Healthcare Hamilton. Hamilton Integrated Research Ethics Board (HIREB #00-1839) approval was obtained prior to beginning the study. Participants gave informed consent to participate in the study before taking part.

**Provenance and peer review** Not commissioned; externally peer reviewed.

**Data availability statement** Data are available upon reasonable request.



**ORCID iDs**
Guillaume Beltramo http://orcid.org/0000-0003-2830-5642
Pierre-Simon Bellaye http://orcid.org/0000-0002-8498-5163

## REFERENCES

1 Wijsenbeek M, Cottin V. Spectrum of fibrotic lung diseases. *N Engl J Med* 2020;383:958–68.
2 Martinez FJ, Collard HR, Pardo A, *et al*. Idiopathic pulmonary fibrosis. *Nat Rev Dis Primers* 2017;3:17074.
3 Nasser M, Larrieu S, Si-Mohamed S, *et al*. Progressive fibrosing interstitial lung disease: a clinical cohort (the PROGRESS study). *Eur Respir J* 2021;57:2002718.
4 Cheng P, Li S, Chen H. Macrophages in lung injury, repair, and fibrosis. *Cells* 2021;10:436.
5 Joshi N, Watanabe S, Verma R, *et al*. A spatially restricted fibrotic niche in pulmonary fibrosis is sustained by M-CSF/M-CSFR signalling in monocyte-derived alveolar macrophages. *Eur Respir J* 2020;55:1900646.
6 Wynn TA, Vannella KM. Macrophages in tissue repair, regeneration, and fibrosis. *Immunity* 2016;44:450–62.
7 Ye Z, Hu Y. TGFbeta1: gentlemanly orchestrator in idiopathic pulmonary fibrosis (review). *Int J Mol Med* 2021;48:132.
8 Gharib SA, Johnston LK, Huizar I, *et al*. MMP28 promotes macrophage polarization toward M2 cells and augments pulmonary fibrosis. *J Leukoc Biol* 2014;95:9–18.
9 Toribio RE, Young N, Schlesinger LS, *et al*. Cy3-tilmanocept labeling of macrophages in joints of mice with antibody-induced arthritis and synovium of human patients with rheumatoid arthritis. *J Orthop Res* 2021;39:821–30.

10 Surasi DS, O'Malley J, Bhambhvani P. 99mTc-Tilmanocept: a novel molecular agent for lymphatic mapping and sentinel lymph node localization. *J Nucl Med Technol* 2015;43:87–91.
11 Azad AK, Rajaram MVS, Metz WL, *et al*. gamma-Tilmanocept, a new radiopharmaceutical tracer for cancer sentinel lymph nodes, binds to the mannose receptor (CD206). *J Immunol* 2015;195:2019–29.
12 Sendo S, Saegusa J, Yamada H, *et al*. Tofacitinib facilitates the expansion of myeloid-derived suppressor cells and ameliorates interstitial lung disease in SKG mice. *Arthritis Res Ther* 2019;21:184.
13 Lescoat A, Lelong M, Jeljeli M, *et al*. Combined anti-fibrotic and anti-inflammatory properties of JAK-inhibitors on macrophages in vitro and in vivo: perspectives for scleroderma-associated interstitial lung disease. *Biochem Pharmacol* 2020;178:114103.
14 Angelidis I, Simon LM, Fernandez IE, *et al*. An atlas of the aging lung mapped by single cell transcriptomics and deep tissue proteomics. *Nat Commun* 2019;10:963.
15 Tanguy J, Goirand F, Bouchard A, *et al*. [$^{18}$F]FMISO PET/CT imaging of hypoxia as a non-invasive biomarker of disease progression and therapy efficacy in a preclinical model of pulmonary fibrosis: comparison with the [$^{18}$F]FDG PET/CT approach. *Eur J Nucl Med Mol Imaging* 2021;48:3058–74.
16 Decologne N, Kolb M, Margetts PJ, *et al*. TGF-beta1 induces progressive pleural scarring and subpleural fibrosis. *J Immunol* 2007;179:6043–51.
17 Han MK, Zhou Y, Murray S, *et al*. Lung microbiome and disease progression in idiopathic pulmonary fibrosis: an analysis of the COMET study. *Lancet Respir Med* 2014;2:548–56.
18 Misharin AV, Morales-Nebreda L, Mutlu GM, *et al*. Flow cytometric analysis of macrophages and dendritic cell subsets in the mouse lung. *Am J Respir Cell Mol Biol* 2013;49:503–10.
19 Byrne AJ, Maher TM, Lloyd CM. Pulmonary macrophages: a new therapeutic pathway in fibrosing lung disease. *Trends Mol Med* 2016;22:303–16.
20 Zhang W, Ohno S, Steer B, *et al*. S100A4 is secreted by alternatively activated alveolar macrophages and promotes activation of lung fibroblasts in pulmonary fibrosis. *Front Immunol* 2018;9:1216.
21 Shi T, Denney L, An H, *et al*. Alveolar and lung interstitial macrophages: definitions, functions, and roles in lung fibrosis. *J Leukoc Biol* 2021;110:107–14.
22 Misharin AV, Morales-Nebreda L, Reyfman PA, *et al*. Monocyte-derived alveolar macrophages drive lung fibrosis and persist in the lung over the life span. *J Exp Med* 2017;214:2387–404.
23 Hamilton RF Jr, Li L, Felder TB, *et al*. Bleomycin induces apoptosis in human alveolar macrophages. *Am J Physiol* 1995;269:L318–25.
24 Joshi N, Walter JM, Misharin AV. Alveolar macrophages. *Cell Immunol* 2018;330:86–90.
25 Zou R, Gui X, Zhang J, *et al*. Association of serum macrophage-mannose receptor CD206 with mortality in idiopathic pulmonary fibrosis. *Int Immunopharmacol* 2020;86:106732.
26 George PM, Spagnolo P, Kreuter M, *et al*. Progressive fibrosing interstitial lung disease: clinical uncertainties, consensus recommendations, and research priorities. *Lancet Respir Med* 2020;8:925–34.
27 Bellamri N, Morzadec C, Joannes A, *et al*. Alteration of human macrophage phenotypes by the anti-fibrotic drug nintedanib. *Int Immunopharmacol* 2019;72:112–23.
28 Ogura T, Taniguchi H, Azuma A, *et al*. Safety and pharmacokinetics of nintedanib and pirfenidone in idiopathic pulmonary fibrosis. *Eur Respir J* 2015;45:1382–92.
29 Wang J, Xu L, Xiang Z, *et al*. Microcystin-LR ameliorates pulmonary fibrosis via modulating CD206(+) M2-like macrophage polarization. *Cell Death Dis* 2020;11:136.
30 Ghebremedhin A, Salam AB, Adu-Addai B, *et al*. A novel CD206 targeting peptide inhibits Bleomycin-induced pulmonary fibrosis in mice. *Cells* 2023;12:1254.
31 Aung WW, Wang C, Xibei J, *et al*. Immunomodulating role of the JAKs inhibitor tofacitinib in a mouse model of bleomycin-induced scleroderma. *J Dermatol Sci* 2021;101:174–84.
32 Dowty ME, Jesson MI, Ghosh S, *et al*. Preclinical to clinical translation of tofacitinib, a Janus kinase inhibitor, in rheumatoid arthritis. *J Pharmacol Exp Ther* 2014;348:165–73.
33 Dhillon S. Tofacitinib: a review in rheumatoid arthritis. *Drugs (Abingdon Engl)* 2017;77:1987–2001.
34 Bergamasco A, Hartmann N, Wallace L, *et al*. Epidemiology of systemic sclerosis and systemic sclerosis-associated interstitial lung disease. *Clin Epidemiol* 2019;11:257–73.
35 Shaw M, Collins BF, Ho LA, *et al*. Rheumatoid arthritis-associated lung disease. *Eur Respir Rev* 2015;24:1–16.
36 Citera G, Mysler E, Madariaga H, *et al*. Incidence rates of interstitial lung disease events in tofacitinib-treated rheumatoid arthritis patients: post hoc analysis from 21 clinical trials. *J Clin Rheumatol* 2021;27:e482–90.
37 Saldarriaga-Rivera LM, López-Villegas VJ. Janus kinase inhibitors as a therapeutic option in rheumatoid arthritis and associated interstitial lung disease. *Rev Colomb Reumatol (Engl Ed)* 2019;26:137–9.
38 Vacchi C, Manfredi A, Cassone G, *et al*. Tofacitinib for the treatment of severe interstitial lung disease related to rheumatoid arthritis. *Case Rep Med* 2021;2021:6652845.
39 Chen Z, Wang X, Ye S. Tofacitinib in amyopathic dermatomyositis-associated interstitial lung disease. *N Engl J Med* 2019;381:291–3.